LETTERS
https://doi.org/10.1038/s41567-020-0931-8

nature physics

Error-corrected gates on an encoded qubit

Philip Reinhold[1,2,3,6]✉, Serge Rosenblum[1,2,4,6]✉, Wen-Long Ma[1,2,5], Luigi Frunzio[1,2], Liang Jiang[1,2,5] and Robert J. Schoelkopf[1,2]✉

To reach their full potential, quantum computers need to be resilient to noise and decoherence. In such a fault-tolerant quantum computer, errors must be corrected in real time to prevent them from propagating between components[1,2]. This requirement is especially pertinent while applying quantum gates, where the interaction between components can cause errors to spread quickly throughout the system. However, the large overhead involved in most fault-tolerant architectures[2,3] makes implementing these systems a daunting task, motivating the search for hardware-efficient alternatives[4,5]. Here, we present a gate enacted by an ancilla transmon on a cavity-encoded logical qubit that is fault-tolerant to ancilla decoherence and compatible with logical error correction. We maintain the purity of the encoded qubit by correcting ancilla-induced errors in real time, yielding a reduction of the logical gate error by a factor of two in the presence of naturally occurring decoherence. We also demonstrate a sixfold suppression of the gate error with increased ancilla relaxation errors and a fourfold suppression with increased ancilla dephasing errors. The results demonstrate that bosonic logical qubits can be controlled by error-prone ancilla qubits without inheriting the ancilla's inferior performance. As such, error-corrected ancilla-enabled gates are an important step towards fault-tolerant processing of bosonic qubits.

In recent years, quantum error correction (QEC) has been demonstrated to protect stored logical qubits against decoherence, either by encoding the information redundantly in a block of multiple physical qubits[6–9] or in a single higher-dimensional bosonic element[10–12]. The concept of fault-tolerant operations extends this principle to the protection of quantum information during a computation involving multiple elements. In particular, errors propagating between elements must not accumulate to the extent that the errors can no longer be removed by QEC. Each task performed in a quantum computer must eventually be made fault-tolerant, including syndrome measurements[13,14], state preparation[14,15] and gates[16]. Only once all the necessary components are realized fault-tolerantly and are connected in a way that is compatible with error correction can one claim a fully fault-tolerant quantum computing architecture with which one could perform computations at any desired accuracy[17].

Some quantum gates are naturally protected by the encoding of choice and do not require additional resources, such as braiding operations in the surface code[3], transversal operations in CSS codes[18] and displacements in GKP codes[19]. However, these 'natural' operations are often insufficient to create a universal gate set[20,21]. One method of addressing this shortcoming is to 'inject' additional gates by coupling to an ancilla qubit that has more complete functionality[22,23]. These ancilla-based operations are not native to the encoding and, as such, require a significant overhead in hardware and number of operations to be implemented fault-tolerantly[2,3].

Here, we devise a hardware-efficient circuit that uses a driven ancilla qubit to apply protected gates to a bosonic logical qubit. Our scheme works by encoding the ancilla in a single multilevel system as well, and using this freedom to identify and correct errors occurring during the gate operation. Remarkably, by employing the information obtained in the final ancilla measurement, we can recover the coherence of the logical qubit and reapply the gate if necessary.

The principal mechanism underlying the gate's fault tolerance is path independence[24]—the property whereby, given fixed initial and final ancilla states, the net logical operation is independent of the specific ancilla trajectory induced by control drives and decoherence events (Fig. 1). Path independence requires that we drive the ancilla in such a way that its populations do not depend on the state of the logical system. Additionally, to make the logical qubit insensitive to the exact timing of ancilla decoherence events, we use an error-transparent interaction[13,25] to couple the ancilla and the qubit.

We implement our logical qubit using a single bosonic mode in a superconducting cavity (Fig. 2a and Supplementary Section 9). Within this mode, quantum information is stored in the subspace defined by the binomial 'kitten' code[26], which, like the Schrödinger cat code[4], can correct for the loss of a single photon. The logical states can be represented in the photon number basis as $|0\rangle_L = \frac{1}{\sqrt{2}}(|0\rangle + |4\rangle)$ and $|1\rangle_L = |2\rangle$. We implement a family of operations $S(\theta) = e^{-i\theta Z_L/2}$, which are rotations by any angle θ around the Z_L axis in the logical subspace (Fig. 2b), using the selective number-dependent arbitrary phase (SNAP) protocol[27,28]. This protocol drives a dispersively coupled transmon ancilla qubit to the excited state with a photon-number-dependent phase. $S(\theta)$ can be effected by choosing the phase of the control drive to be zero on photon number states $|0\rangle$ and $|4\rangle$, and θ on $|2\rangle$. The arbitrary angle of rotation in $S(\theta)$ allows the realization of logical Clifford operations ($\theta = k\pi/2$, with $k \in \mathbb{Z}$) as well as non-Clifford operations such as the T-gate ($\theta = \pi/4$). This gate set can be combined with a single rotation around a different logical axis to provide universal control of the logical qubit.

The ancilla undergoes two predominant types of error: dephasing and energy relaxation. To correct the effects of these errors, we must first make them independently detectable. We do so by modifying the SNAP protocol to use three levels of the ancilla, instead of two. By driving a Raman transition (Fig. 2c and Supplementary Section 5) from the ground state ($|g\rangle$) to the second excited state ($|f\rangle$) with a photon-number-dependent phase, we implement the SNAP operation while avoiding population of the first excited state ($|e\rangle$). Next, we swap $|f\rangle$ and $|g\rangle$ so as to minimize the probability of

[1]Department of Applied Physics and Physics, Yale University, New Haven, CT, USA. [2]Yale Quantum Institute, Yale University, New Haven, CT, USA. [3]Present address: HRL Laboratories, LLC, Malibu, CA, USA. [4]Present address: Department of Condensed Matter Physics, Weizmann Institute of Science, Rehovot, Israel. [5]Present address: Pritzker School of Molecular Engineering, University of Chicago, Chicago, IL, USA. [6]These authors contributed equally: Philip Reinhold, Serge Rosenblum. ✉e-mail: pcreinhold@hrl.com; serge.rosenblum@weizmann.ac.il; robert.schoelkopf@yale.edu

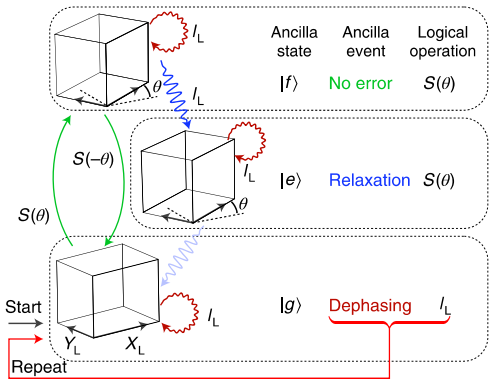

Fig. 1 | Working principle of the error-corrected logical gate. Control drives excite the ancilla from the ground state $|g\rangle$ to the second excited state $|f\rangle$ around an axis $e^{i\phi}|f\rangle\langle g| + e^{-i\phi}|g\rangle\langle f|$ with $\phi = \theta$ for the logical state $|1\rangle_L$ and $\phi = 0$ for $|0\rangle_L$. This implements the gate $S(\theta)$ (green arrows), which represents a Z_L rotation by an angle θ on the logical system (boxes). Path independence requires that all closed loops in the ancilla transition graph produce the identity operation on the logical qubit, implying that the logical operation is uniquely determined by a measurement of the ancilla state (Supplementary Section 2). A rapid, unconditional *gf* swap (shown in Fig. 2d) is applied before the measurement to minimize the probability of ancilla relaxation during the measurement. Error transparency guarantees that the logical operation associated with the dominant decoherence events (ancilla relaxation and dephasing, depicted by blue and dark red arrows) is the identity I_L. The operation succeeds in the case of either no error or relaxation. In the case of dephasing, the operation is not applied, but repeating the protocol makes the gate succeed deterministically. Relaxation from $|e\rangle$ to $|g\rangle$, shown with a faint arrow, breaks path independence, as well as error transparency, but is a low-probability second-order error.

ancilla relaxation during the subsequent ancilla state measurement (Fig. 2d and Supplementary Section 7). The measurement outcome determines which (if any) type of ancilla error occurred, as well as the operation effected on the cavity state.

We ensure protection against ancilla dephasing during the SNAP operation by simultaneously driving the ancilla to $|f\rangle$ with equal rates Ω for all photon number states in the logical subspace. Because the control drives have photon-number-dependent phases, the ancilla becomes entangled with the logical system. However, in the limit of driving slowly compared to the dispersive coupling, the ancilla population remains uncorrelated with the logical state during the driven evolution (Supplementary Section 5). Therefore, projecting the ancilla to $|g\rangle$ or $|f\rangle$ at any time during the protocol, as the environment does in the case of dephasing, does not impart any back-action on the logical state. However, dephasing events will create some probability of not successfully finishing the transit from $|g\rangle$ to $|f\rangle$. By considering the effective Hamiltonian in the interaction picture during the operation (Supplementary Section 1)

$$H_{\mathrm{int}} = \Omega\, S(\theta) \otimes |f\rangle\langle g| + \Omega^*\, S(-\theta) \otimes |g\rangle\langle f| \qquad (1)$$

we can see that the logical action associated with going from $|g\rangle$ to $|f\rangle$ is the desired gate $S(\theta)$, whereas the logical action of going from $|f\rangle$ to $|g\rangle$ is the inverse operation $S(-\theta)$. As a result, if the ancilla trajectory ends in $|g\rangle$ ($|f\rangle$ following the final swap) due to a dephasing event, the net effect on the logical system is the identity operation. Remarkably, this path independence ensures protection even against multiple dephasing events. We can ensure deterministic application of the gate in the presence of dephasing by resetting the ancilla and repeating the protocol upon measuring $|f\rangle$.

Energy relaxation during application of the gate occurs predominantly through decay from $|f\rangle$ to $|e\rangle$. The latter state remains unaffected under the action of the control drives, and therefore the final state should be detected as $|e\rangle$, assuming no further decay events. Because the trajectory taking the ancilla from $|g\rangle$ to $|e\rangle$ passes through $|f\rangle$ (Fig. 1), the effective operation on the logical system is $S(\theta)$. However, the cavity state will also acquire a random phase-space rotation (depending on the jump time) due to the static cavity–ancilla interaction $\chi_{fe}|f\rangle\langle f|a^\dagger a$, where $a^\dagger a$ is the photon-number operator and χ_{fe} the dispersive interaction rate in $|f\rangle$ in a frame rotating with $|e\rangle$. This random rotation can be understood as the back-action induced by the emitted ancilla excitation carrying photon-number-dependent energy. By using the detuned sideband driving scheme presented in ref. [13], we can effectively set $\chi_{fe} = 0$ for the duration of the gate (Supplementary Section 6). This 'error-transparency' drive eliminates the random rotation imparted on the cavity state, thereby maintaining path independence in the case of relaxation.

In addition to ancilla errors, the protocol is compatible with QEC protecting against photon loss in the cavity. Because the control drives do not act on the system in the odd photon number subspace, the result is equivalent to incomplete driving followed by photon loss. Although not done in this work, applying a parity measurement[13,29] and recovery operation[26] following the protocol would make the effect of photon loss equivalent to that of ancilla dephasing (Supplementary Section 3).

The key feature here is that, regardless of the measured ancilla state, the cavity remains in a definite pure state contained within the logical subspace. To demonstrate this, we create[30] the state $|+X\rangle_L = \frac{1}{\sqrt{2}}(|0\rangle_L + |1\rangle_L)$, apply the operation $S(\pi/2)$ and perform Wigner tomography (Fig. 2c). In this experiment, the error-transparency drive is applied and the ancilla is measured without conditional repetition of the gate. The Wigner functions are shown separately for each measured ancilla state. To emphasize the effect of ancilla errors, we increase the ancilla error probability during this operation (Supplementary Section 4), so that the probabilities of relaxation and dephasing errors are ~20% each. As expected, in the case of successful completion of the protocol (ancilla in $|g\rangle$), or in the case of relaxation (ancilla in $|e\rangle$), the gate is correctly applied. Different deterministic phase-space rotations are acquired by the cavity for different final ancilla states as a result of evolution during the ancilla measurement. This angle can be corrected in software by updating the phase of subsequent drives around the cavity resonance frequency. Finally, in the case of ancilla dephasing (ancilla in $|f\rangle$), we observe the initial logical state $|+X\rangle_L$. The slight asymmetry is a result of the Kerr evolution, whose removal requires successful completion of the logical gate[28].

We next perform two versions of the full gate, the standard (non-corrected) gate S_{NC} and the error-corrected gate S_C (Fig. 2d), again with increased ancilla error rates. We characterize the result via Wigner tomography without conditioning on the ancilla measurement outcome (Fig. 2e). In the case of the standard gate (S_{NC}), we observe significant smearing of the final state. However, in the case of the error-corrected gate (S_C), which includes the error-transparency drive, ancilla measurement, reset and conditional repetition, it is evident that, despite the high ancilla error rate, the cavity coherence is mostly preserved.

To establish the gate's logical error probability quantitatively, we turn to interleaved randomized benchmarking (IRB)[31]. We first create a set of operations from the logical Clifford group using numerical optimal control[30]. We then interleave the $S(\pi/2)$ gate between randomly selected Clifford operations, scanning the length of the sequence (Fig. 3a). We measure the probability of obtaining the correct answer in the ancilla after applying a decoding operation as a function of the sequence length n (Fig. 3b), and compare the performance of S_{NC} and S_C. The measured gate error probability for

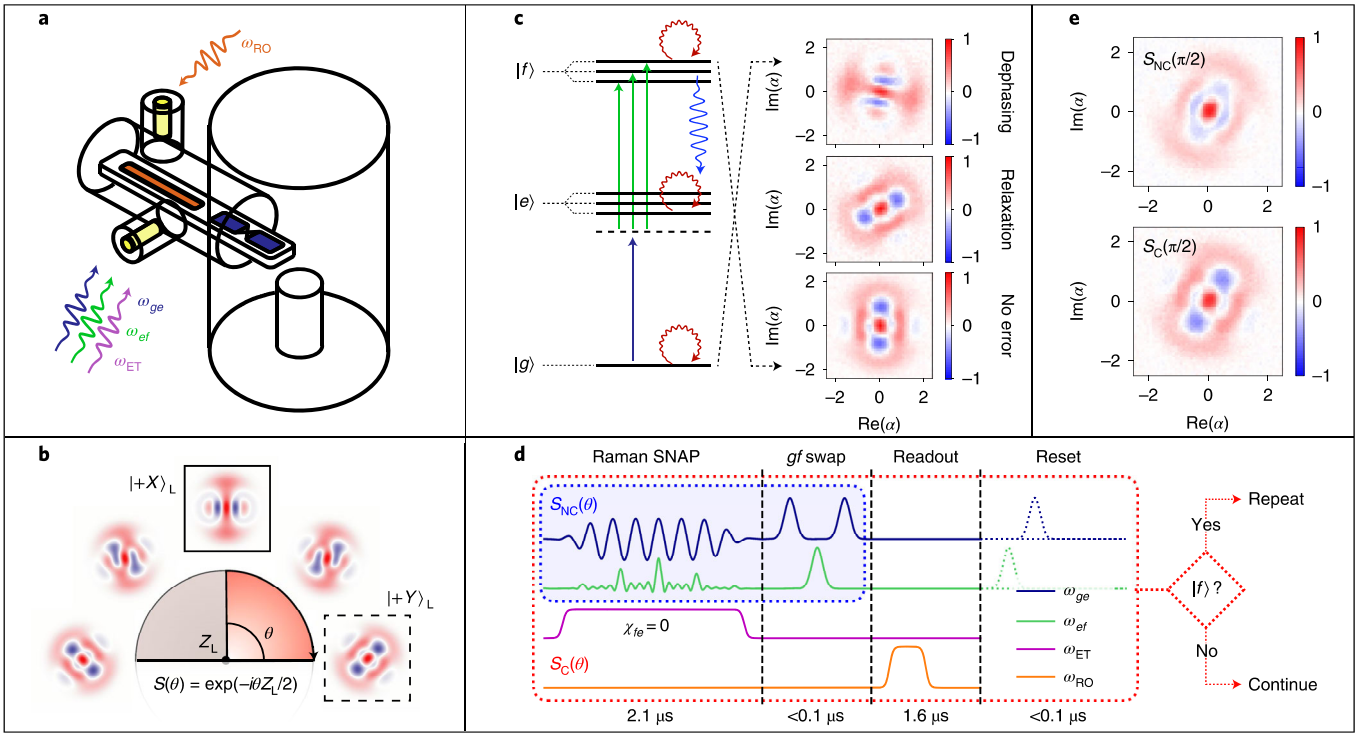

Fig. 2 | Experimental protocol and tomography of logical states after gate application. a, The system consists of a $\lambda/4$ coaxial superconducting cavity coupled to an ancilla transmon (blue), which is in turn coupled to a stripline readout resonator (orange). The protocol involves control drives, which address the first (ω_{ge}) and second (ω_{ef}) ancilla transition frequencies off-resonantly, the error-transparency drive (at ω_{ET}, Supplementary Section 6)[13] and the readout drive (ω_{RO}). **b**, The protocol effects a rotation around the logical Z_L axis by an arbitrary amount θ. In the following demonstrations, we prepare the initial state $|+X\rangle_L$ (simulated Wigner function in the solid box) using numerically optimized pulses of duration 1.2 µs, and apply a $\theta = \pi/2$ rotation, producing the target state $|+Y\rangle_L$ (dashed box). **c**, The Raman SNAP operation consists of applying a control drive detuned from the ω_{ge} transition (blue arrow) as well as a comb of control drives (green arrows), detuned in the opposite sense from the ω_{ef} transition and separated in frequency by twice the ancilla-cavity dispersive shift $2\chi_{fg} = 2\pi \times -2.4$ MHz (Supplementary Section 5). The measured Wigner tomograms of the cavity state, post-selected on the final ancilla state following a *gf* swap (dashed arrows), are shown to the right. The different cavity phase-space rotations are a result of state-dependent Stark shifts during the ancilla measurement. **d**, The control sequence without error correction ($S_{NC}(\theta)$, blue box) involves the Raman SNAP operation and a *gf* swap (Supplementary Section 7), and takes 2.2 µs. In the error-corrected protocol ($S_C(\theta)$, red box), we add the error-transparency drive during the SNAP operation to remove the random cavity phase-space rotation induced by $|f\rangle \rightarrow |e\rangle$ relaxation. We then add an ancilla readout and reset (taking 1.6 µs, including feedback latency), and reapply all steps upon measuring $|f\rangle$. **e**, Unconditional Wigner tomogram after application of the logical gate without error correction (top) and with error correction (bottom). When applying the error-corrected logical gate, ancilla-state-dependent rotations of the cavity phase space are corrected in software. The data in this figure were obtained with artificially induced ancilla dephasing and relaxation probabilities (~20% each) to emphasize the increase in the fidelity of the final state when error correction is performed.

S_{NC} (obtained from the difference between the decay rates of the interleaved and the non-interleaved sequences) is $4.6 \pm 0.1\%$. The main effect in producing this error probability is ancilla relaxation (~2.5%), with an additional 0.8% resulting from ancilla dephasing, photon loss and thermal ancilla excitation. In contrast, the error-corrected gate has an error probability of $2.4 \pm 0.1\%$. No single process dominates the remaining error, but a full accounting of the known sources, including photon loss, readout-induced dephasing and other sources predicts an error probability of 2.1% (Supplementary Section 8). Incorporating photon-loss error correction and reducing ancilla readout times (without inducing cavity dephasing[32]) would provide the most impactful reductions in the logical error rate.

To demonstrate the robustness of the gate to ancilla decoherence, we intentionally introduce noise to increase the ancilla dephasing and relaxation rates (Supplementary Section 4). We scan the induced *gf* dephasing rate and *ef* relaxation rates from their native rates of 1/(40 µs) and 1/(47 µs), respectively, up to maximum rates of ~1/(2 µs). The measured ancilla state probabilities vary as expected, with P_e changing from 3.4% to 25% with increased relaxation rate and P_f changing from <1% to 14% with increased dephasing rate (Fig. 3c). For S_{NC}, the induced gate error probability is nearly equal to the probability of measuring the ancilla in an excited state, indicating that ancilla errors are bound to propagate and affect the logical qubit. However, for S_C, the ratio of gate errors to ancilla errors (Supplementary Section 4) is suppressed by a factor of 5.8 ± 0.2 (4.2 ± 0.4) for injected *ef* relaxation (*gf* dephasing) errors, clearly demonstrating the resilience of the gate against dominant ancilla errors.

The error-corrected gate is readily extended to protect against a broader class of ancilla errors, such as thermal excitation or multiple-decay events, by employing higher ancilla levels. Furthermore, we can incorporate protection against photon loss by performing a fault-tolerant parity measurement[13] after the gate, and using the result to perform QEC[10]. Recently, a different type of gate on a bosonic logical qubit was demonstrated to be error-transparent to photon loss errors[33]. We have demonstrated the feasibility of a hardware-efficient approach to protecting quantum information not only during storage, but also as it is being processed by quantum gates. Expanding these results to create additional error-corrected

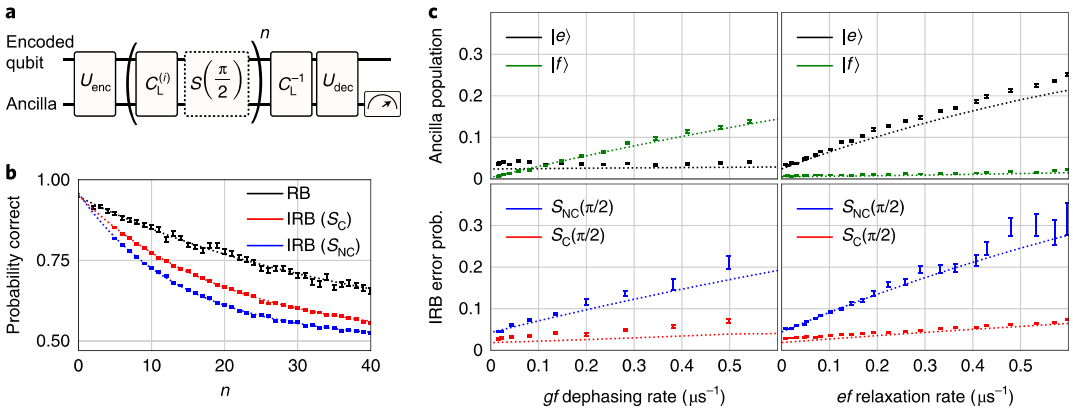

Fig. 3 | Benchmarking of the logical gate. a, Circuit for randomized benchmarking (RB) and interleaved randomized benchmarking (IRB)[30]. We first prepare an encoded state of the cavity using a numerically optimized encoding pulse U_{enc}. Next, we perform a random sequence of n operations drawn from the Clifford group, $C_L^{(i)}$. In the interleaved variants, after each random Clifford, we apply the logical gate (dashed box), either using the non-error-corrected (S_{NC}) or error-corrected (S_C) protocol. Finally, the net inverse Clifford operation is applied, followed by a decoding operation U_{dec}. This maps the encoded information onto the ancilla, where it can be measured. **b**, By fitting both the RB and IRB results to an exponential model $Ae^{-\gamma n} + \frac{1}{2}$ (dotted lines), we can learn the effective gate error probability. Without interleaved logical gates, we measure $\gamma_{RB} = 2.5 \pm 0.1\%$ (black). We can determine the error probability associated with the error-corrected (non-error-corrected) operation as $\gamma_{IRB} - \gamma_{RB} = 2.4 \pm 0.1\%$ ($4.6 \pm 0.1\%$) from the red (blue) curve. **c**, To demonstrate the robustness of the protocol, we add noise to the system (Supplementary Section 4), which has the effect of increasing either the ancilla dephasing (left) or relaxation rates (right). We measure the ancilla population (top) and IRB-inferred error probabilities (bottom). We see that the populations are affected nearly independently by the respective noise parameters. We also see that, in both cases, S_C (red markers) is significantly less likely than S_{NC} (blue markers) to translate ancilla errors induced by the added noise into logical errors. The dotted lines are derived from a full quantum simulation using independently measured system parameters. Error bars indicate standard deviations.

gates[34,35] and therefore providing universal fault-tolerant control, is a promising path towards robust quantum computing devices.

Online content

Any methods, additional references, Nature Research reporting summaries, source data, extended data, supplementary information, acknowledgements, peer review information; details of author contributions and competing interests; and statements of data and code availability are available at https://doi.org/10.1038/s41567-020-0931-8.

Received: 4 December 2019; Accepted: 4 May 2020;
Published online: 8 June 2020

References

1. Preskill, J. Fault-tolerant quantum computation. In *Introduction to Quantum Computation and Information* (ed. Lo, H.-K.) 213–269 (World Scientific, 1998).
2. Campbell, E. T., Terhal, B. M. & Vuillot, C. Roads towards fault-tolerant universal quantum computation. *Nature* **549**, 172–179 (2017).
3. Fowler, A. G., Mariantoni, M., Martinis, J. M. & Cleland, A. N. Surface codes: towards practical large-scale quantum computation. *Phys. Rev. A* **86**, 032324 (2012).
4. Mirrahimi, M. et al. Dynamically protected cat-qubits: a new paradigm for universal quantum computation. *New J. Phys.* **16**, 045014 (2014).
5. Guillaud, J. & Mirrahimi, M. Repetition cat qubits for fault-tolerant quantum computation. *Phys. Rev. X* **91**, 041053 (2019).
6. Kelly, J. et al. State preservation by repetitive error detection in a superconducting quantum circuit. *Nature* **519**, 66–69 (2015).
7. Nigg, D. et al. Quantum computations on a topologically encoded qubit. *Science* **345**, 302–305 (2014).
8. Cramer, J. et al. Repeated quantum error correction on a continuously encoded qubit by real-time feedback. *Nat. Commun.* **7**, 11526 (2016).
9. Córcoles, A. et al. Demonstration of a quantum error detection code using a square lattice of four superconducting qubits. *Nat. Commun.* **6**, 6979 (2015).
10. Ofek, N. et al. Extending the lifetime of a quantum bit with error correction in superconducting circuits. *Nature* **536**, 441–445 (2016).
11. Flühmann, C. et al. Encoding a qubit in a trapped-ion mechanical oscillator. *Nature* **566**, 513–517 (2019).
12. Hu, L. et al. Quantum error correction and universal gate set operation on a binomial bosonic logical qubit. *Nat. Phys.* **15**, 503–508 (2019).
13. Rosenblum, S. et al. Fault-tolerant detection of a quantum error. *Science* **361**, 266–270 (2018).
14. Linke, N. M. et al. Fault-tolerant quantum error detection. *Sci. Adv.* **3**, e1701074 (2017).
15. Takita, M., Cross, A. W., Córcoles, A. D., Chow, J. M. & Gambetta, J. M. Experimental demonstration of fault-tolerant state preparation with superconducting qubits. *Phys. Rev. Lett.* **119**, 180501 (2017).
16. Harper, R. & Flammia, S. T. Fault-tolerant logical gates in the IBM quantum experience. *Phys. Rev. Lett.* **122**, 080504 (2019).
17. Aharonov, D. & Ben-Or, M. Fault-tolerant quantum computation with constant error rate. *SIAM J. Comput.* **38**, 1207–1282 (2008).
18. Steane, A. M. & Ibinson, B. Fault-tolerant logical gate networks for Calderbank–Shor–Steane codes. *Phys. Rev. A* **72**, 052335 (2005).
19. Gottesman, D., Kitaev, A. & Preskill, J. Encoding a qubit in an oscillator. *Phys. Rev. A* **64**, 012310 (2001).
20. Eastin, B. & Knill, E. Restrictions on transversal encoded quantum gate sets. *Phys. Rev. Lett.* **102**, 110502 (2009).
21. Webster, P. & Bartlett, S. D. Braiding defects in topological stabiliser codes of any dimension cannot be universal. Preprint at https://arxiv.org/pdf/1811.11789.pdf (2018).
22. Bravyi, S. & Kitaev, A. Universal quantum computation with ideal Clifford gates and noisy ancillas. *Phys. Rev. A* **71**, 022316 (2005).
23. Zhou, X., Leung, D. W. & Chuang, I. L. Methodology for quantum logic gate construction. *Phys. Rev. A* **62**, 052316 (2000).
24. Ma, W.-L. et al. Path independent quantum gates with noisy ancilla. Preprint at https://arxiv.org/pdf/1911.12240.pdf (2019).
25. Kapit, E. Error-transparent quantum gates for small logical qubit architectures. *Phys. Rev. Lett.* **120**, 050503 (2018).
26. Michael, M. H. et al. New class of quantum error-correcting codes for a bosonic mode. *Phys. Rev. X* **6**, 031006 (2016).
27. Krastanov, S. et al. Universal control of an oscillator with dispersive coupling to a qubit. *Phys. Rev. A* **92**, 040303 (2015).
28. Heeres, R. W. et al. Cavity state manipulation using photon-number selective phase gates. *Phys. Rev. Lett.* **115**, 137002 (2015).
29. Sun, L. et al. Tracking photon jumps with repeated quantum non-demolition parity measurements. *Nature* **511**, 444–448 (2014).
30. Heeres, R. W. et al. Implementing a universal gate set on a logical qubit encoded in an oscillator. *Nat. Commun.* **8**, 94 (2017).
31. Magesan, E. et al. Efficient measurement of quantum gate error by interleaved randomized benchmarking. *Phys. Rev. Lett.* **109**, 080505 (2012).
32. Touzard, S. et al. Gated conditional displacement readout of superconducting qubits. *Phys. Rev. Lett.* **122**, 080502 (2019).

33. Ma, Y. et al. Error-transparent operations on a logical qubit protected by quantum error correction. *Nat. Phys.* https://doi.org/10.1038/s41567-020-0893-x (2020).
34. Xu, Y. et al. Demonstration of controlled-phase gates between two error-correctable photonic qubits. *Phys. Rev. Lett.* **124**, 120501 (2020).
35. Gao, Y. Y. et al. Entanglement of bosonic modes through an engineered exchange interaction. *Nature* **566**, 509–512 (2019).

Data availability

The data that support the findings of this study are available from the corresponding authors upon reasonable request.

Acknowledgements

We thank N. Frattini and K. Sliwa for providing the Josephson parametric converter and N. Ofek for providing the logic for the field programmable gate array used for the control of this experiment. We thank M. Zhang and Y. Wong for helpful discussions. S.R., L.F. and R.J.S. acknowledge funding support from the US Army Research Office (W911NF-18-1-0212). P.R. and S.R. were supported by the Air Force Office of Scientific Research (FA9550-15-1-0015 and FA9550-14-1-0052).

Author contributions

P.R. and S.R. fabricated the transmon qubits, assembled the experimental apparatus, performed the experiments and analysed the data under the supervision of L.F. and R.J.S. W.-L.M. and L.J. provided theoretical support. P.R., S.R. and R.J.S. wrote the manuscript with feedback from all authors.

Competing interests

L.F. and R.J.S. are co-founders of, and equity shareholders in, Quantum Circuits, Inc. S.R., P.R., L.J., L.F. and R.J.S. are inventors on patent application no. 62/613,974 submitted by Yale University, which covers hardware-efficient fault-tolerant operations with superconducting circuits.

Additional information

Supplementary information is available for this paper at https://doi.org/10.1038/s41567-020-0931-8.

Correspondence and requests for materials should be addressed to P.R., S.R. or R.J.S.

Peer review information *Nature Physics* thanks Tanay Roy and the other, anonymous, reviewer(s) for their contribution to the peer review of this work.